ACS Photonics
pubs.acs.org/journal/apchd5 Letter

Electrical Tuning of Fresnel Lens in Reflection

Christopher Damgaard-Carstensen,* Martin Thomaschewski, Fei Ding, and Sergey I. Bozhevolnyi*

Cite This: ACS Photonics 2021, 8, 1576−1581
Read Online
ACCESS | Metrics & More | Article Recommendations | Supporting Information

ABSTRACT: Optical metasurfaces have been extensively investigated, demonstrating diverse and multiple functionalities with complete control over the transmitted and reflected fields. Most optical metasurfaces are, however, static, with only a few configurations offering (rather limited) electrical control, thereby jeopardizing their application prospects in emerging flat optics technologies. Here, we suggest an approach to realize electrically tunable optical metasurfaces, demonstrating dynamic Fresnel lens focusing. The active Fresnel lens (AFL) exploits the electro-optic Pockels effect in a 300 nm thick lithium niobate layer sandwiched between a continuous thick and a nanostructured gold film serving as electrodes. We fabricate and characterize the AFL, focusing 800−900 nm radiation at a distance of 40 μm, with the focusing efficiency of 15%, and demonstrating the modulation depth of 1.5%, with the driving voltage of ±10 V within the bandwidth of ∼6.4 MHz. We believe that the electro-optic metasurface concept introduced is useful for designing dynamic flat optics components.

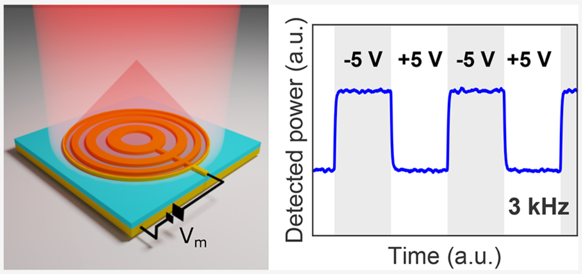

KEYWORDS: *metasurface, flat optics, electrical tunability, lithium niobate, Fresnel lens*

Over the past decade, optical metasurfaces, representing nm-thin planar arrays of resonant subwavelength elements, have been extensively investigated, demonstrating diverse and multiple functionalities that make use of the available complete control over the transmitted and reflected fields.[1−4] This progress led to the realization of numerous flat optical components in concert with the current trend of miniaturization in photonics. Large flexibility in the design of optical metasurfaces enabled numerous demonstrations of various functionalities, including beam-steering,[5−7] optical holograms,[8−10] and planar lenses.[11−13] Most of the developed optical metasurfaces are however static, featuring well-defined optical responses determined by the configuration of material and geometrical parameters that are chosen by design and set in the process of fabrication. Realization of dynamic metasurfaces faces formidable challenges associated with the circumstance that metasurfaces are fundamentally very thin, that is, of subwavelength thickness, thereby severely limiting the interaction length available. Efficient tunability can be achieved through material property (phase) transitions or structural reconfigurations that result in very large refractive index changes, but these effects are inherently slow.[14−17] The speed limitations jeopardize the application prospects in emerging technologies, such as light detection and ranging (LIDAR) and computational imaging and sensing.[18,19]

The electro-optic Pockels effect enables fast electrically controlled modulation of material properties in several active media, for example, lithium niobate (LN), electro-optic polymers, or aluminum nitride.[20−22] Especially LN offers an attractive platform, due to its large electro-optic coefficients (r_{33} = 31.45 pm/V), preserved also at elevated temperatures due to a very large Curie temperature (∼1200 °C), superb chemical and mechanical stability resulting in long-term reliability, and wide optical transparency range (0.35−4.5 μm).[23] The aforementioned limitations in the available interaction length makes, however, exploiting comparatively weak electro-optic material effects problematic, resulting in rather weak tunability and modulation efficiency.[21,24]

We introduce in this work an approach to realize electrically tunable optical metasurfaces by utilizing the electro-optic effect in a thin LN layer sandwiched between a continuous thick bottom and nanostructured top gold film serving as electrodes. Our approach is based on electrically tuning the light reflectivity near a high-fidelity Fabry−Perot resonance. This concept is implemented in dynamic (electrically controlled) Fresnel lens focusing. By conducting detailed numerical simulations and experiments for a 300 nm thick LN layer, we demonstrate that the active Fresnel lens (AFL) exhibits tunable focusing and modulation in reflection at near-infrared wavelengths. The fabricated AFL is found to exhibit focusing of 800−900 nm radiation at the distance of 40 μm with the focusing efficiency of 15% and modulation depth of 1.5% (for the driving voltage of ±10 V) within the bandwidth of ∼6.4 MHz. We believe that the introduced electro-optic metasurface concept is useful for designing dynamic flat optics components.

Received: April 6, 2021
Published: June 1, 2021

■ RESULTS AND DISCUSSION

Figure 1 shows schematics of the proposed structure consisting of semitransparent gold rings deposited on a continuous $t_{LN} \simeq$ 300 nm z-cut LN thin film, adhered to a 300 nm optically thick gold back-reflector by a 10 nm chromium adhesive layer. The areas covered by semitransparent gold constitute Fabry−Perot resonators, whose resonances determine the operation wavelength of the device. The two-dimensional (2D) Fresnel lenses allow polarization-independent focusing, due to their radial symmetry. For simplicity the polarization is set to be along the x-direction, denoted TM polarization. In the design of a Fresnel lens, the relation between wavelength, focal length, and lens dimension is given by $r_m = \sqrt{m\lambda f + \frac{1}{4}m^2\lambda^2}$, where λ is the wavelength of light to be focused, f is the focal length, m is an integer describing the zones, and r_m is the radius of the m^{th} zone. The focal length is a key parameter in the design of a zone plate, and to realize a tight focal spot, a focal length of 40 μm is selected in combination with a wavelength range of 800−900 nm and a total of m_{Tot} = 19 zones. This results in a total zone plate radius of $r_{19} \simeq 26\,\mu$m, and a minimum zone width of $\Delta r_{19} \simeq 0.75\,\mu$m.

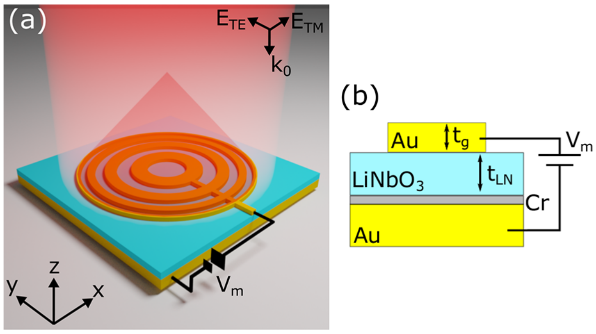

Figure 1. Schematics of the designed active Fresnel lens (AFL). (a) Three dimensional rendering of the zone plate showing focusing of the incident light under an applied voltage. (b) Cross section sketch displaying a semitransparent gold ring deposited on a lithium niobate thin film, adhered to a gold back-reflector by a thin chromium adhesive layer.

The concentric gold rings and the gold back-reflector can serve as integrated metal electrodes for electro-optic tuning of the Fresnel lens (Figure 1). The concentric rings of the Fresnel lens are electrically connected by a 2 μm wide wire (Figure 1a). Applying a voltage across the gold rings and the bottom back-reflector electrode generates an electric field in the sandwiched LN thin film, which induces a change of the refractive index due to the Pockels effect. This shifts the resonance position of the Fabry−Perot resonators, thus, giving rise to electrical tunability of the light reflectivity. With the Fabry−Perot optical mode propagating along the z-direction, the optical electric field component effectively influencing the Fabry−Perot resonance is in the x-direction, thus the relevant electro-optic Pockels coefficient is r_{13} = 10.12 pm/V.[25] The induced change in refractive index is given by $|\Delta n| \simeq \frac{r}{2}n_0^3\frac{V}{d}$, where r is the relevant Pockels coefficient, n_0 is the refractive index, V is the applied voltage, and d is the distance across which the voltage is applied.[26] To realize an effective AFL, the modulation and reflective properties of the Fabry−Perot resonators are investigated to determine the optimal thickness of the top concentric gold rings, leading to the choice of using a thickness of t_g = 15 nm (see Supporting Information, section 1).

An important characteristic of a focusing element is the focusing efficiency, describing the amount of incident light that is directed to the designed focal spot. Another equally important characteristic when discussing active optical components is the modulation efficiency (calculated as $1 - (|I_{\min}(\lambda)|/|I_{\max}(\lambda)|)$, where $|I_{\min}(\lambda)|$ and $|I_{\max}(\lambda)|$ are the minimum and maximum achievable intensity at the focal spot for a given wavelength, respectively[27]), namely, the ability to modulate the device performance by applying an external voltage. In this work, we optimize the design to achieve the highest possible modulation efficiency. Given the previously mentioned design parameters, the only parameter left to optimize is the design wavelength, which for optimal modulation is determined by calculating the focusing and modulation efficiency as a function of design wavelength, meaning that the zone plate design is adjusted at each iteration

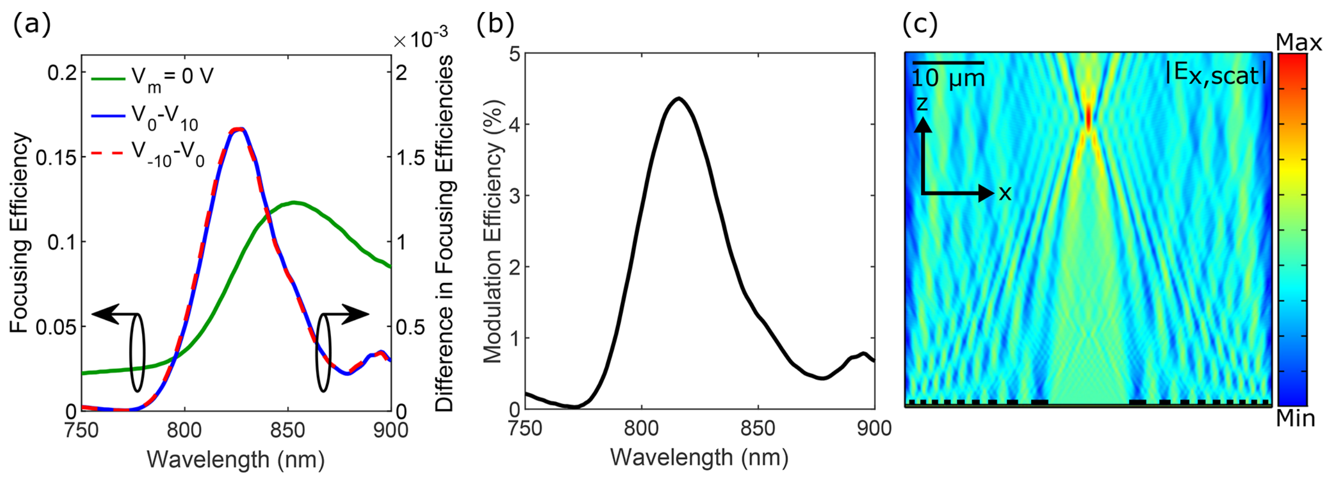

Figure 2. Calculated performance of the AFL. (a) Calculated focusing efficiency (left axis) as a function of wavelength without an applied modulation voltage, and variation in focusing efficiency (right axis) when applying a DC modulation voltage of ±10 V. (b) Calculated modulation of the focusing efficiency as a function of wavelength, when applying a DC modulation voltage of ±10 V (c) Calculated x-component of the scattered field above an AFL with a designed focal length of 40 μm at an incident wavelength of 815 nm for a DC modulation voltage of −10 V.

https://doi.org/10.1021/acsphotonics.1c00520
ACS Photonics 2021, 8, 1576−1581

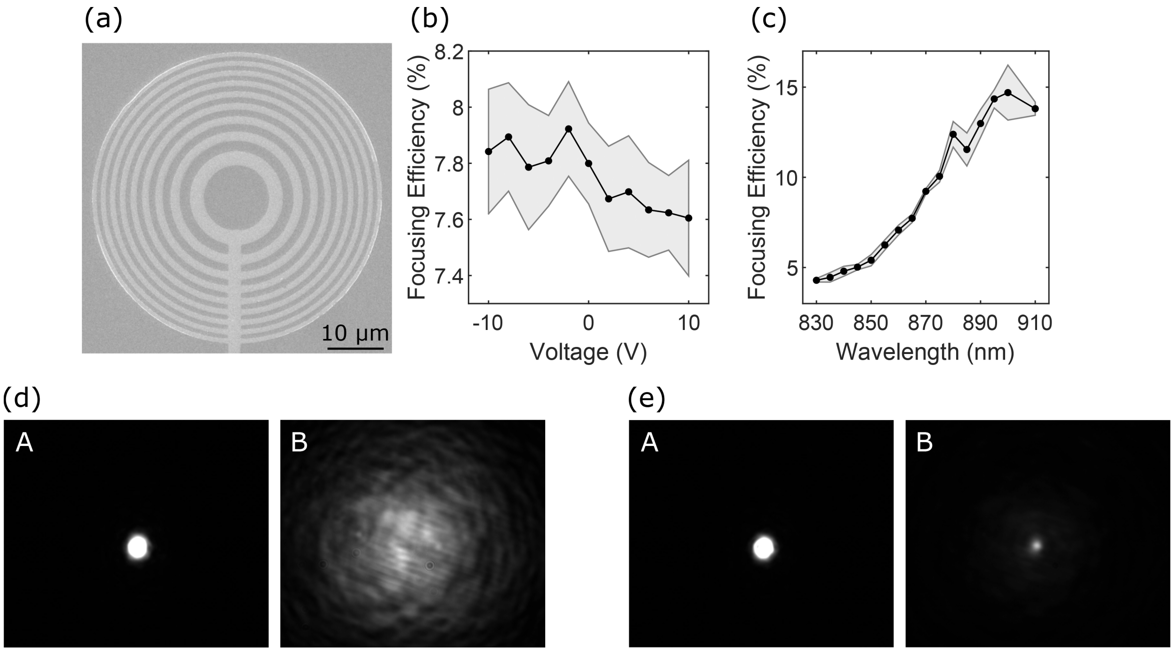

Figure 3. Experimental characterization of the focusing effect of the AFL. (a) Scanning electron microscopy image of the fabricated AFL. (b, c) Verification of the (b) electrical and (c) spectral tunability of the focal spot intensity as a function of DC modulation voltage for a wavelength of 865 nm and of wavelength for a DC modulation voltage of −10 V, respectively. The shaded error region represents the linearly interpolated standard deviation of the mean deduced from repeated measurements. (d, e) Optical images in planes A and B (Supporting Information, Figure S4) when the incident light of wavelength 865 nm illuminate (d) flat unstructured gold and (e) the fabricated AFL, respectively.

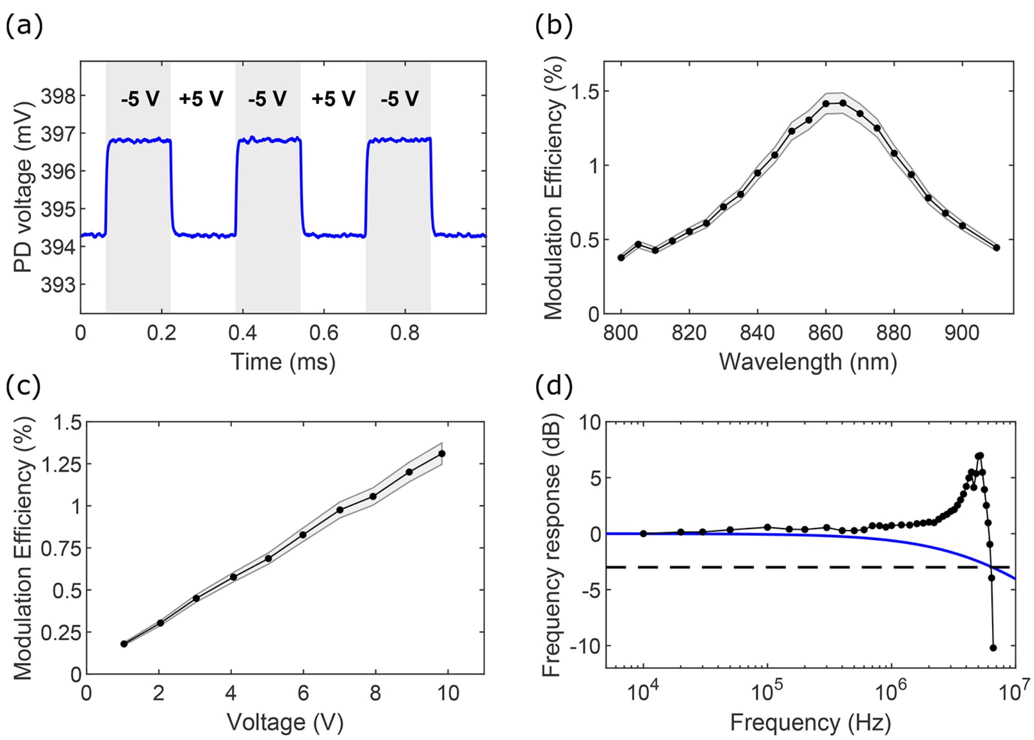

Figure 4. Experimental characterization of the modulation performance of the AFL. (a) Intensity in the focal spot, measured with the photodetector (PD), as a function of time for a wavelength of 865 nm, while the modulation voltage is cycled between −5 and 5 V, indicated by gray and white backgrounds, respectively. (b) Measured modulation efficiency of the intensity in the focal spot as a function of wavelength for a modulation voltage of ±10 V at a frequency of 3 kHz. The shaded error region represents the linearly interpolated estimated standard deviation of the mean. (c) Measured modulation efficiency as a function of modulation voltage for a wavelength of 865 nm at a frequency of 3 kHz. Indicated voltages represent amplitudes of the applied signal. The shaded error region represents the linearly interpolated estimated standard deviation of the mean. (d) Measured frequency response as a function of applied RF signal frequency, normalized to the lowest applied frequency, at a wavelength of 865 nm. The dashed line marks −3 dB, and the blue line represents the response of a first order low pass filter with a cutoff frequency of 6.5 MHz, which is calculated as the cutoff of the macroscopic electrodes. Error bars are in the order of data point sizes.

https://doi.org/10.1021/acsphotonics.1c00520
ACS Photonics 2021, 8, 1576−1581

of the wavelength (Supporting Information, Figure S3). Simulations show that the focusing efficiency increases significantly from ∼3 to ∼20% in the investigated wavelength range (see Supporting Information, section 2). The design wavelength is chosen to be at the point of maximum modulation efficiency, thus, λ_0 = 815 nm. Similar simulations are performed for varying incident wavelengths, but with a constant lens design (Figure 2). The performance is equivalent in the vicinity of the design wavelength, and the most significant distinction is for the focusing efficiency at longer wavelengths, where the performance loss due to mismatch between the incident and design wavelengths overcomes the otherwise increasing focusing efficiency. The largest differences in focusing efficiencies are observed at the part of steepest slope. The shape of the curve for modulation efficiency resembles those for difference in focusing efficiencies, only slightly blue-shifted, because the modulation efficiency is calculated based on the difference relative to the unmodulated signal. Note that variations in the refractive index due to the electro-optic Pockels effect are very small and linear. Therefore, changes in the focusing efficiency and thus the modulation efficiency are proportional to the applied voltage within the considered voltage range and can be deduced from the results specified at ±10 V. Figure 2c shows a scattered field simulation of the investigated AFL at the design wavelength illustrating the focusing ability.

After thorough numerical investigations of the AFL performance, we move on to experimental characterization. An AFL with the chosen design parameters was fabricated using the standard technological procedure based on electron-beam lithography (see Methods). A scanning electron microscopy image of the AFL is shown in Figure 3a, showing regular concentric circles without significant fabrication defects. Due to the expected short focal length of the AFL and the relatively low focusing efficiency, it proved difficult to characterize the focusing effect using a conventional imaging setup with near-parallel illumination,[11] because the focal point will be difficult to distinguish from the interference pattern between incident and normally reflected light from the sample. However, it is possible to verify the focusing effect and determine the focal length by shifting the sample away from the objective from the plane which resulted in a tight focal spot under illumination of flat unstructured gold (plane A in Supporting Information, Figure S4) into the plane where the reflected light from the AFL is tightly focused (plane B in Supporting Information, Figure S4).[13,28] It is deducible from geometrical optics that the distance between these planes is equivalent to twice the focal length. This approach of positioning the sample in planes A and B for radiation incident on flat unstructured gold and the fabricated AFL produces optical images as shown in Figure 3d,e, respectively, clearly demonstrating the focusing ability.

Experimental characterization of the Fabry−Perot modulator shows a measured thickness of the LN thin film of 323 nm (see Supporting Information, section 1). This corresponds to a deviation of ∼7.5% of the nominal thickness, which results in a shift in resonant wavelength of approximately 50 nm. For this reason we see a new wavelength for highest modulation of 865 nm (Figure 4b), which is used as the central wavelength for experimental characterization. This is expected to result in a decrease in performance, as the lens is designed for a wavelength of 815 nm. The measured focal length is f = (40 ± 2) μm. Focusing efficiency is investigated as a function of modulation voltage and wavelength (Figure 3b,c). The measured and calculated values are not directly comparable as the simulations are for a 2D model. However, the simulations provide trends in the performance for varying voltage and wavelength, which are comparable to the experiments. As is shown by simulations (Figure 2a), applying a negative (positive) bias results in an increase (decrease) in focusing efficiency, which is verified by experiments (Figure 3b). Similarly, the evolution of focusing efficiency with wavelength (Figure 3c) follows that shown by simulations (Figure 2a).

So far, we have characterized the focusing abilities of the AFL, and now we move on to characterize the modulation properties of the intensity in the focal spot (see Methods). The ability to modulate the focal point intensity is visualized by applying an electrical square signal alternating between ±5 V. Measured response of the AFL at an electrical frequency of 3 kHz shows the dynamic modulation of focusing versus time and demonstrates as previously stated that a negative bias leads to an increase in focusing efficiency (Figure 4a). Modulation efficiency is measured at a driving voltage of ±10 V for the wavelength range of 800−910 nm (Figure 4b). The maximum modulation efficiency of 1.5% is measured at a wavelength of 865 nm, and the measured dispersion of the modulation efficiency is in agreement with the simulated wavelength dependence (Figure 2b). The modulation efficiency can be improved by selecting materials with larger electro-optic coefficients, such as electro-optic polymers and barium titanate offering electro-optic Pockels coefficients on the order of $r_{33} \geq$ 100 pm/V.[29,30] However, both materials suffer from relatively low thermal stability with structural phase transitions occurring at temperatures around 100 °C. As previously stated, the linear electro-optic Pockels effect results in proportionality in our case when applying reasonable voltages. This proportionality extends to the modulation efficiency, which will increase proportionally for reasonable increases in the electro-optic Pockels coefficient. A linear relation is expected between modulation efficiency and voltage due to the previously stated formula for induced refractive index change, and the resulting shift in the wavelength of Fabry−Perot resonance. This relation is verified by experimental characterization (Figure 4c). The electro-optic frequency response is characterized from 10 kHz to 7 MHz (Figure 4d). The device frequency response exhibits an increase in performance for larger signal frequency before abruptly dropping, resulting in a −3 dB cutoff frequency of 6.4 MHz. Frequency response fluctuations might be attributed to piezoelectric resonances in LN, and the accompanied variations of the permittivity and the electro-optic activity in LN when the crystal strain becomes unable to follow the external electric field (clamped crystal response).[20,25,31] The capacitance of the device is measured to be 0.49 nF, and assuming a 50 Ω resistive load ($f = 1/[2\pi RC]$), the calculated −3 dB cutoff frequency is 6.5 MHz, which is indicated by a first order low pass filter response (blue line of Figure 4d), intersecting the measured data at the −3 dB line. Disregarding the macroscopic electrodes and electrical wiring and using a simple parallel plate capacitor formula, the capacitance of the device is calculated to be 0.83 pF, resulting in a cutoff frequency of 3.8 GHz, which is easily supported by the fast electro-optic Pockels effect. Thus, the electrical bandwidth can be considerably improved by optimizing the electrode configuration and limiting the bottom electrode to a

https://doi.org/10.1021/acsphotonics.1c00520
ACS Photonics 2021, 8, 1576−1581

circular area corresponding to the size of and located just below the patterned Fresnel lens.

CONCLUSION

In summary, we have presented and experimentally investigated an approach to realize a flat electrically tunable Fresnel lens by utilizing the electro-optic effect in a thin lithium niobate layer sandwiched between a continuous thick bottom and nanostructured top gold film serving as electrodes. We have designed, fabricated and characterized the active Fresnel lens that exhibits focusing of 800−900 nm radiation at the distance of 40 μm with the focusing efficiency of 15% and modulation depth of 1.5% for the driving voltage of ±10 V within the bandwidth of 6.4 MHz. It should be noted that the modulation efficiency can significantly be improved by using a high-quality top gold film with the optimal thickness of 12 nm (see Supporting Information, section 1), as the currently used 15 nm thin gold film is likely to be inhomogeneous (island-like). Furthermore, redesigning the bottom electrode can considerably improve the electrical bandwidth reaching the GHz range as discussed above. In comparison with other electrically tunable thin lenses,[15−17] the configuration presented here is attractive due to its simplicity in design and fabrication and inherently fast electro-optic response (see Supporting Information, section 4). Overall, we believe the introduced electro-optic metasurface concept is useful for designing dynamic, electrically tunable flat optics components.

METHODS

Modeling. Simulations are performed in the commercially available finite element software *COMSOL Multiphysics*, ver. 5.5. Fabry−Perot modulators and Fresnel lenses are modeled to determine reflectivity and focusing properties. All simulations are performed for 2D models due to computational restraints. In all setups, the incident wave is a plane wave traveling downward, normal to the sample. Interpolated experimental values are used for the permittivity of gold,[32] LN,[33] and chromium,[34] and the medium above the sample is air. For the simulation of the Fabry−Perot modulators, periodic boundary conditions are applied on both sides of the cell, while the top and bottom boundaries are truncated by ports to minimize reflections. The top port, positioned a distance of one wavelength from the top electrode, handles wave excitation and measures a complex reflection coefficient. For the simulation of the AFL, periodic boundary conditions are applied on one side, so it is only necessary to model half the zone plate. All other boundaries are truncated by scattering boundary conditions, also to eliminate reflections. Focusing efficiency is determined by integrating the reflected power over an area corresponding to twice the beam waist of a Gaussian beam focused at the focal point and dividing by the incident optical power.

Fabrication. Fabrication of the AFL is done using a combination of nanostenciling and electron beam lithography and lift-off. A substrate with the following custom material stack is obtained: LN substrate, 3 μm of SiO_2, 30 nm of chromium, 300 nm of gold, 10 nm of chromium, and a 300 nm thin film of LN (NANOLN). Initially, macroscopic electrodes are deposited by thermal evaporation of 3 nm titanium and 50 nm gold through a shadow mask. Subsequently, ∼200 nm of PMMA 950 K A4 is spin-coated, and the Fresnel zones and modulator squares are exposed at 30 kV using electron beam lithography. Alignment between the macroscopic electrodes and optical devices is performed manually. After development, the devices are formulated by thermal evaporation of 1 nm titanium and 15 nm gold followed by lift-off in acetone. The fabricated modulator squares are 100 μm × 100 μm, and the AFL has a radius of 26.1 μm and consists of 19 zones, with even zones formed by gold deposition.

Electro-Optical Characterization. During fabrication, the concentric rings are interfaced to macroscopic electrodes. For electro-optical characterization, the sample is mounted on a homemade sample holder, that connects to the macroscopic top electrode, and electrical connection to the bottom electrode is obtained by applying a conductive paste on the edge of the sample. The incident light is a low power, continuous-wave laser beam from a tunable laser, which is focused by a 50× objective to form a tightly focused spot in plane A (Supporting Information, Figure S4) on flat unstructured gold. The reflected light is collected by the same objective, separated from the incident light by a beam splitter and viewed on a camera. Focusing efficiency is determined as the ratio of focused light from the device viewed in plane B to the amount of reflected light on flat unstructured gold viewed in plane A. For characterization of the modulation properties, the focal spot is manually isolated with an iris and the camera is replaced with a photodetector connected to an oscilloscope. RF modulation signals are supplied by a function generator, and modulation of the focal spot intensity is observed on the oscilloscope.

ASSOCIATED CONTENT

Supporting Information

The Supporting Information is available free of charge at https://pubs.acs.org/doi/10.1021/acsphotonics.1c00520.

Investigation of the Fabry−Perot modulator, determination of the design wavelength, setup for electro-optical characterization, and comparison of electrically tunable thin lenses (PDF)

AUTHOR INFORMATION

Corresponding Authors

Christopher Damgaard-Carstensen − *Centre for Nano Optics, University of Southern Denmark, DK-5230 Odense M, Denmark;* orcid.org/0000-0001-7087-0798; Email: cdc@mci.sdu.dk

Sergey I. Bozhevolnyi − *Centre for Nano Optics, University of Southern Denmark, DK-5230 Odense M, Denmark;* orcid.org/0000-0002-0393-4859; Email: seib@mci.sdu.dk

Authors

Martin Thomaschewski − *Centre for Nano Optics, University of Southern Denmark, DK-5230 Odense M, Denmark;* orcid.org/0000-0003-2545-1468

Fei Ding − *Centre for Nano Optics, University of Southern Denmark, DK-5230 Odense M, Denmark;* orcid.org/0000-0001-7362-519X

Complete contact information is available at: https://pubs.acs.org/10.1021/acsphotonics.1c00520

Author Contributions

S.I.B. conceived the idea. C.D.-C. designed the sample and performed the numerical simulations with F.D. C.D.-C. and

M.T. fabricated the structures and conducted the electro-optical characterization. C.D.-C. analyzed the results, which were discussed by all authors. C.D.-C. and S.I.B. wrote the manuscript with revisions by all authors. S.I.B. supervised the project.

Notes

The authors declare no competing financial interest.

■ ACKNOWLEDGMENTS

The authors are thankful for financial support from Villum Fonden (Award in Technical and Natural Sciences 2019 and Grant Nos. 00022988 and 37372). C.D.-C. acknowledges advice from Chao Meng on the optical characterization of focusing devices.

■ REFERENCES

(1) Yu, N.; Genevet, P.; Kats, M. A.; Aieta, F.; Tetienne, J.-P.; Capasso, F.; Gaburro, Z. Light Propagation with Phase Discontinuities: Generalized Laws of Reflection and Refraction. *Science* **2011**, *334*, 333−337.

(2) Hsiao, H.-H.; Chu, C. H.; Tsai, D. P. Fundamentals and Applications of Metasurfaces. *Small Methods* **2017**, *1*, 1600064.

(3) Chen, H.-T.; Taylor, A. J.; Yu, N. A review of metasurfaces: physics and applications. *Rep. Prog. Phys.* **2016**, *79*, 076401.

(4) Ding, F.; Pors, A.; Bozhevolnyi, S. I. Gradient metasurfaces: a review of fundamentals and applications. *Rep. Prog. Phys.* **2018**, *81*, 026401.

(5) Pors, A.; Albrektsen, O.; Radko, I. P.; Bozhevolnyi, S. I. Gap plasmon-based metasurfaces for total control of reflected light. *Sci. Rep.* **2013**, *3*, 2155.

(6) Li, Z.; Palacios, E.; Butun, S.; Aydin, K. Visible-Frequency Metasurfaces for Broadband Anomalous Reflection and High-Efficiency Spectrum Splitting. *Nano Lett.* **2015**, *15*, 1615−1621.

(7) Damgaard-Carstensen, C.; Ding, F.; Meng, C.; Bozhevolnyi, S. I. Demonstration of $>2\pi$ reflection phase range in optical metasurfaces based on detuned gap-surface plasmon resonators. *Sci. Rep.* **2020**, *10*, 19031.

(8) Chen, W. T.; Yang, K.-Y.; Wang, C.-M.; Huang, Y.-W.; Sun, G.; Chiang, I.-D.; Liao, C. Y.; Hsu, W.-L.; Lin, H. T.; Sun, S.; Zhou, L.; Liu, A. Q.; Tsai, D. P. High-Efficiency Broadband Meta-Hologram with Polarization-Controlled Dual Images. *Nano Lett.* **2014**, *14*, 225−230.

(9) Wen, D.; Yue, F.; Li, G.; Zheng, G.; Chan, K.; Chen, S.; Chen, M.; Li, K. F.; Wong, P. W. H.; Cheah, K. W.; Yue Bun Pun, E.; Zhang, S.; Chen, X. Helicity multiplexed broadband metasurface holograms. *Nat. Commun.* **2015**, *6*, 8241.

(10) Huang, Y.-W.; Chen, W. T.; Tsai, W.-Y.; Wu, P. C.; Wang, C.-M.; Sun, G.; Tsai, D. P. Aluminum Plasmonic Multicolor Meta-Hologram. *Nano Lett.* **2015**, *15*, 3122−3127.

(11) Ding, F.; Chen, Y.; Yang, Y.; Bozhevolnyi, S. I. Multifunctional Metamirrors for Broadband Focused Vector-Beam Generation. *Adv. Opt. Mater.* **2019**, *7*, 1900724.

(12) Yi, H.; Qu, S.-W.; Chen, B.-J.; Bai, X.; Ng, K. B.; Chan, C. H. Flat Terahertz Reflective Focusing Metasurface with Scanning Ability. *Sci. Rep.* **2017**, *7*, 3478.

(13) Boroviks, S.; Deshpande, R. A.; Mortensen, N. A.; Bozhevolnyi, S. I. Multifunctional Metamirror: Polarization Splitting and Focusing. *ACS Photonics* **2018**, *5*, 1648−1653.

(14) Che, Y.; Wang, X.; Song, Q.; Zhu, Y.; Xiao, S. Tunable optical metasurfaces enabled by multiple modulation mechanisms. *Nanophotonics* **2020**, *9*, 4407−4431.

(15) van de Groep, J.; Song, J.-H.; Celano, U.; Li, Q.; Kik, P. G.; Brongersma, M. L. Exciton resonance tuning of an atomically thin lens. *Nat. Photonics* **2020**, *14*, 426−430.

(16) Park, S.; Lee, G.; Park, B.; Seo, Y.; bin Park, C.; Chun, Y. T.; Joo, C.; Rho, J.; Kim, J. M.; Hone, J.; Jun, S. C. Electrically focus-tuneable ultrathin lens for high-resolution square subpixels. *Light: Sci. Appl.* **2020**, *9*, 98.

(17) Shirmanesh, G. K.; Sokhoyan, R.; Wu, P. C.; Atwater, H. A. Electro-optically Tunable Multifunctional Metasurfaces. *ACS Nano* **2020**, *14*, 6912−6920.

(18) Schwarz, B. Mapping the world in 3D. *Nat. Photonics* **2010**, *4*, 429−430.

(19) Jung, I. W.; Lopez, D.; Qiu, Z.; Piyawattanametha, W. 2-D MEMS Scanner for Handheld Multispectral Dual-Axis Confocal Microscopes. *J. Microelectromech. Syst.* **2018**, *27*, 605−612.

(20) Thomaschewski, M.; Zenin, V. A.; Wolff, C.; Bozhevolnyi, S. I. Plasmonic monolithic lithium niobate directional coupler switches. *Nat. Commun.* **2020**, *11*, 748.

(21) Zhang, J.; Kosugi, Y.; Otomo, A.; Ho, Y.-L.; Delaunay, J.-J.; Nakano, Y.; Tanemura, T. Electrical tuning of metal-insulator-metal metasurface with electro-optic polymer. *Appl. Phys. Lett.* **2018**, *113*, 231102.

(22) Smolyaninov, A.; El Amili, A.; Vallini, F.; Pappert, S.; Fainman, Y. Programmable plasmonic phase modulation of free-space wavefronts at gigahertz rates. *Nat. Photonics* **2019**, *13*, 431−435.

(23) Weis, R. S.; Gaylord, T. K. Lithium niobate: Summary of physical properties and crystal structure. *Appl. Phys. A: Solids Surf.* **1985**, *37*, 191−203.

(24) Gao, B.; Ren, M.; Wu, W.; Cai, W.; Xu, J. Electro-optic lithium niobate metasurfaces. *Sci. China: Phys., Mech. Astron.* **2021**, *64*, 240362.

(25) Jazbinšek, M.; Zgonik, M. Material tensor parameters of $LiNbO_3$ relevant for electro- and elasto-optics. *Appl. Phys. B: Lasers Opt.* **2002**, *74*, 407−414.

(26) Pedrotti, F. L.; Pedrotti, L. M.; Pedrotti, L. S. *Introduction to Optics*, 3rd ed.; Pearson Education Limited, 2014.

(27) Yao, Y.; Shankar, R.; Kats, M. A.; Song, Y.; Kong, J.; Loncar, M.; Capasso, F. Electrically Tunable Metasurface Perfect Absorbers for Ultrathin Mid-Infrared Optical Modulators. *Nano Lett.* **2014**, *14*, 6526−6532.

(28) Pors, A.; Nielsen, M. G.; Eriksen, R. L.; Bozhevolnyi, S. I. Broadband Focusing Flat Mirrors Based on Plasmonic Gradient Metasurfaces. *Nano Lett.* **2013**, *13*, 829−834.

(29) Abel, S.; et al. Large Pockels effect in micro- and nanostructured barium titanate integrated on silicon. *Nat. Mater.* **2019**, *18*, 42−47.

(30) Ayata, M.; Fedoryshyn, Y.; Heni, W.; Baeuerle, B.; Josten, A.; Zahner, M.; Koch, U.; Salamin, Y.; Hoessbacher, C.; Haffner, C.; Elder, D. L.; Dalton, L. R.; Leuthold, J. High-speed plasmonic modulator in a single metal layer. *Science* **2017**, *358*, 630−632.

(31) Takeda, K.; Hoshina, T.; Takeda, H.; Tsurumi, T. Electro-optic effect of lithium niobate in piezoelectric resonance. *J. Appl. Phys.* **2012**, *112*, 124105.

(32) Johnson, P. B.; Christy, R. W. Optical Constants of the Noble Metals. *Phys. Rev. B* **1972**, *6*, 4370−4379.

(33) Zelmon, D. E.; Small, D. L.; Jundt, D. Infrared corrected Sellmeier coefficients for congruently grown lithium niobate and 5 mol% magnesium oxide − doped lithium niobate. *J. Opt. Soc. Am. B* **1997**, *14*, 3319.

(34) Johnson, P.; Christy, R. Optical constants of transition metals: Ti, V, Cr, Mn, Fe, Co, Ni, and Pd. *Phys. Rev. B* **1974**, *9*, 5056−5070.

https://doi.org/10.1021/acsphotonics.1c00520
ACS Photonics 2021, 8, 1576−1581

Supporting Information for Electrical Tuning of Fresnel Lens in Reflection

Christopher Damgaard-Carstensen*, Martin Thomaschewski, Fei Ding, and Sergey I. Bozhevolnyi*

Centre for Nano Optics, University of Southern Denmark, Campusvej 55, DK-5230 Odense M, Denmark

*To whom correspondence should be addressed:

cdc@mci.sdu.dk, seib@mci.sdu.dk

Number of pages: 6

Number of figures: 4

Number of tables: 1

1 Investigation of the Fabry-Perot modulator

The design of the proposed active Fresnel lens (AFL) requires an in-depth understanding of the Fabry-Perot resonators constituting the active part of our device (Figure S1a). We wish to operate the resonator around resonance to be able to tune the reflective properties. The resonance is achieved by obtaining destructive interference between the light reflected from the bottom and top gold electrode layers. Thus, it is necessary to match the reflected power from each layer and assure they are out of phase. The phase change is primarily acquired through the difference in optical path length between the two reflection channels, and it is therefore controlled by the thickness of the lithium niobate (LN) layer and the wavelength of the incident light. The reflected power is matched by appropriately selecting the thickness of the top gold layer. As mentioned in the main text, the thickness of the LN layer is $t_{LN} \simeq 300\,\text{nm}$, and hence the important design parameters of the resonator are the thickness of the top gold layer and the wavelength. An amplitude map is composed by varying the top electrode thickness and incident wavelength (Figure S1b). A resonance is clearly visible at a wavelength of $\sim 840\,\text{nm}$ and a thickness of $\sim 10\,\text{nm}$. Our work is aimed at achieving maximum modulation efficiency, which is calculated for a DC modulation voltage of $\pm 10\,\text{V}$, and shows a sharp maximum at a thickness of $t_g = 12\,\text{nm}$ (Figure S1c). The maximum is relatively sharp due to the rather small shift of the resonance under the applied modulation voltage. Optimizing for highest modulation efficiency, we should use a top electrode thickness of $t_g = 12\,\text{nm}$ (Figure S1d), however this poses some problems in fabrication. Experience shows that the minimum realizable film thickness, in order to achieve a homogeneous thin film, is 15 nm with the equipment at hand. This results in a less pronounced resonance, and thus a reduction in achievable modulation efficiency by a factor of five (Figure S1d,e), yet reliability of the homogeneity of the gold film is paramount for the experimental realization leading to the choice of using a top electrode thickness of 15 nm.

After numerical investigations, we move on to experimental characterization. Using standard electron-beam lithography and lift-off, the Fabry-Perot modulator is realized by fabricating a square with dimensions $100\,\mu\text{m} \times 100\,\mu\text{m}$, which is connected to a macroscopic electrode by a $2\,\mu\text{m}$ wide stripe, in order to establish electrical connection. A scanning electron microscopy image of the square is shown in Figure S2a. Quantification of the modulator performance is carried out by comparison of the modulation efficiency determined through both simulation and experimental characterization (Figure S2b). An incident beam is limited to the square by an iris, and the modulation properties are measured when applying a modulation voltage of $\pm 10\,\text{V}$ (see Methods section of the main text). The measured data show a shifted resonance compared to the previously calculated data (Figure S1e and S2b), which is primarily due to variation in the thickness of the LN thin film. Based on the measured data, an adjusted thickness of 323 nm is determined by matching the spectral position of the resonance. The obtained results show good correspondence between the shapes of the curves, although the measured

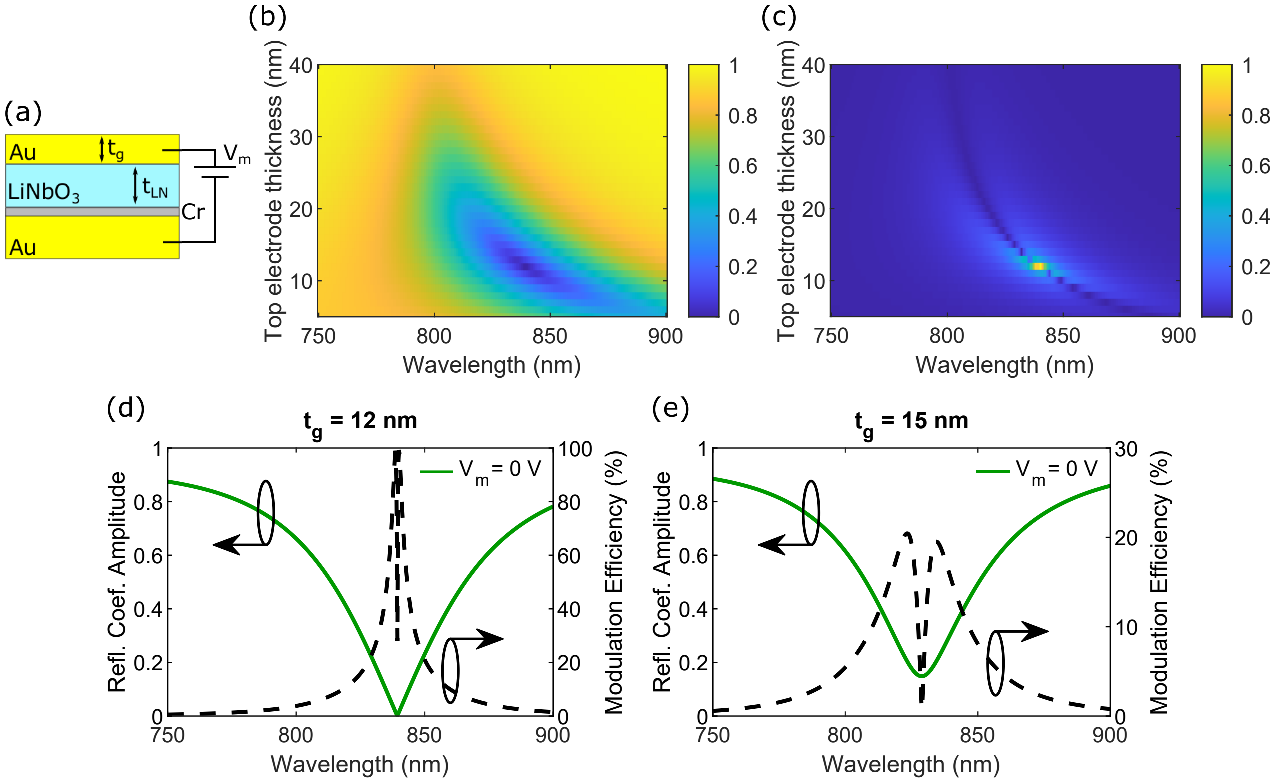

Figure S1: Calculated performance of a Fabry-Perot modulator. (a) Cross section sketch displaying the semi-transparent gold layer deposited on a lithium niobate thin film, adhered to a gold back-reflector by a thin chromium adhesive layer. (b) Calculated reflection coefficient amplitude as a function of thickness of the top gold layer and wavelength of the normally incident light. (c) Calculated modulation efficiency as a function of thickness of the top gold layer and wavelength for DC modulation voltages of ±10 V. (d,e) Plots of reflection coefficient amplitude (left axis) and modulation efficiency (right axis) versus wavelength for a thickness of the top gold layer of (d) $t_g = 12$ nm and (e) $t_g = 15$ nm at DC modulation voltages of ±10 V.

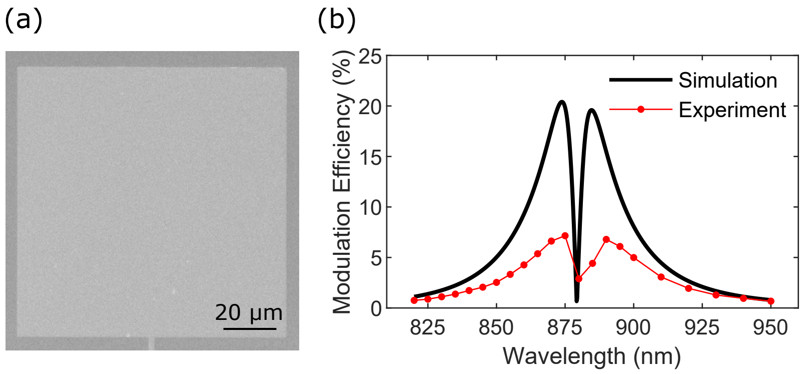

Figure S2: Experimental characterization of a Fabry-Perot modulator. (a) Scanning electron microscopy image of a gold square of 100 μm × 100 μm used for characterization of the modulator. (b) Calculated and measured modulation efficiency of the modulator as a function of wavelength for a modulation voltage of ±10 V. Error bars are in the order of data point sizes. The thickness of the lithium niobate thin film for calculation of the modulation efficiency is adjusted to match the resonance of the measured data. This results in an adjusted thickness of 323 nm.

modulation efficiency is a factor of two lower than the calculated one. We believe these additional losses are due to various factors, including absorption in the titanium adhesion layer or inhomogeneity in the semitransparent gold thin film, yet we achieve significantly higher modulation efficiencies than those obtained with a similar structure using electro-optic polymers [1].

2 Determination of design wavelength

After having determined the optimal thickness of the top gold electrode, we wish to determine the design wavelength leading to maximum modulation of the intensity in the focal spot. To do so, wavelength dependence of the focusing efficiency is simulated for DC modulation voltages of 0 and ±10 V for a lens design that is updated for each iteration of the wavelength (Figure S3a). A significant increase in focusing efficiency from ∼3 to ∼20 % is present in the investigated wavelength range, and the largest difference in focusing efficiency, due to the applied modulation voltage, occurs at the part of steepest slope. Comparing to Figure S1e, the maximum focusing efficiency is achieved far from the Fabry-Perot resonance of the resonator. The reason for this is found in the phase response (Figure S3c). Focusing from a Fresnel lens in reflection can be achieved in two ways: By eliminating reflected light from each alternating zone, or by assuring the reflected light from alternating zones is out of phase. We design the AFL using the first approach, thus alternating reflective and absorbing zones, because this allows for modulation of the focal spot intensity by tuning the reflectivity of the absorbing zones. However, this approach limits the maximum achievable focusing efficiency, as much of the incident light is absorbed. The phase response of the Fabry-Perot resonator shows that at the wavelength of 950 nm, corresponding to maximum focusing efficiency, the incident light experiences a phase shift of ∼ 180° from the resonator compared to areas without top gold electrodes, thus causing the AFL to focus using the second approach leading to increased focusing efficiency. Investigation of the graphs

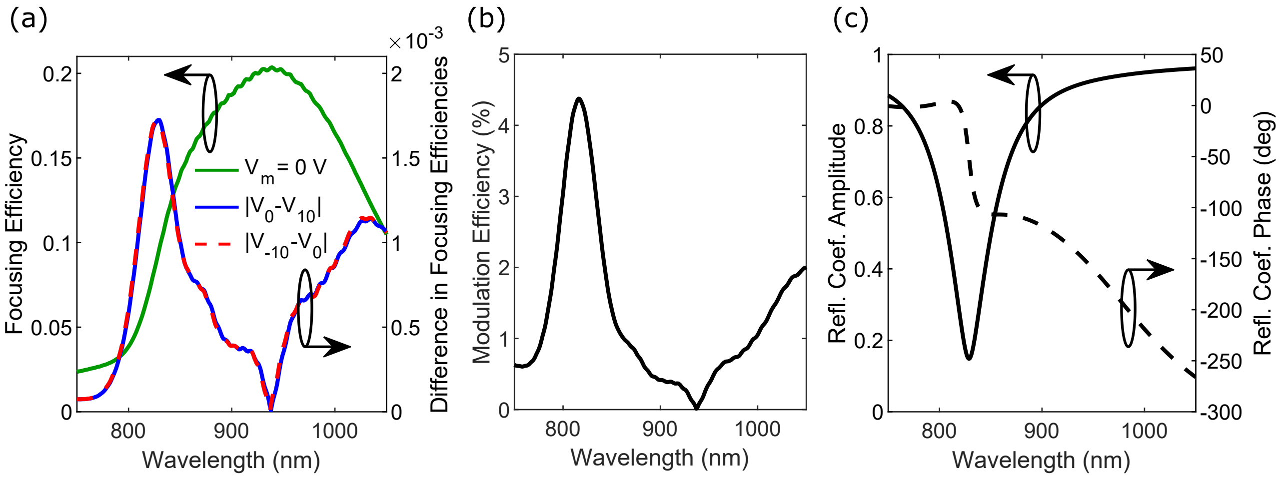

Figure S3: Determining the optimal Fresnel lens design wavelength. (a,b) The investigated lens dimensions are updated for each iteration of the incident wavelength. (a) Calculated focusing efficiency (left axis) as a function of wavelength for no modulation voltage, and variation in focusing efficiency (right axis) when applying DC modulation voltages of ±10 V. (b) Calculated modulation of the focusing efficiency as a function of wavelength, when applying DC modulation voltages of ±10 V. (c) Investigation of the evolution of reflection coefficient amplitude and reflected phase with wavelength for the Fabry-Perot resonator.

(Figure S3a,b), show, however, that the maximum in focusing efficiency comes with a minimum in modulation efficiency, thus resulting in the choice of a design wavelength of 815 nm, which points to the largest modulation efficiency at the cost of lower focusing efficiency.

3 Electro-optical characterization of the AFL

The fabricated AFL is characterized using a setup similar to those previously used for characterizing focusing metasurfaces (Figure S4) [2, 3]. An incident low-power continuous wave laser beam is focused to a spot on flat unstructured gold (plane A in Figure S4) by a long working distance 50X objective. The focusing effect of the AFL is visualized by shifting the sample a distance of $2f$ to the plane where the reflected light is tightly focused (plane B in Figure S4). Reflected light is separated from the incident light by a beam splitter and viewed on a camera or photodetector depending on which characteristic is under investigation (see Methods section of the main text).

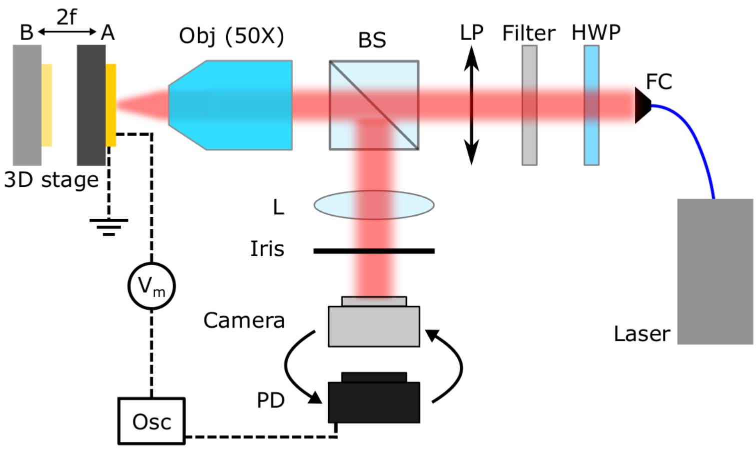

Figure S4: Schematic of the optical setup used for characterization of the AFL. The optical path is indicated by red while the electrical wiring is indicated by black dashed lines. A and B represent two planes, separated by a distance of twice the focal length, where the incident light and reflected light from the AFL produce a focused spot, respectively. FC: Fiber-coupling, HWP: Half-wave plate, LP: Linear polarizer, L: Lens, BS: Beam splitter, Obj: Objective, PD: Photodetector, Osc: Oscilloscope, V_m: Modulation voltage source.

4 Comparison of electrically tunable thin lenses

	Ref. [4]	Ref. [5]	Ref. [6]	**Our work**
Focusing efficiency	65 %	2 % (BSt)	0.06 %	**15 %**
Modulation efficiency	-	-	33 %	**1.5 %**
Wavelength range (nm)	445 – 630	1500 – 1530	550 – 650	**800 – 900**
Modulation voltage (V)	±50	±6	+3	**±10**
Electrical bandwidth	-	-	< 25 Hz*	**6.4 MHz**
Possibility for reconfiguration	Dynamic control of focal length	Dynamic beam steering or focusing	-	**-**
Ease of fabrication	FIB	Multi-step lithography	Multi-step lithography	**One-step lithography**
Material platform	Multilayer graphene	ITO	WS_2/ graphene	**LN**

*Estimation from rise/fall times

Table S1: Comparison of recently published works on electrically tunable thin lenses with our work, comparing several key characteristics. Abbreviations are: BSt: Beam steering, FIB: Focused ion beam milling, ITO: Indium tin oxide, WS_2: Tungsten disulfide, LN: Lithium niobate

References

[1] Zhang, J.; Kosugi, Y.; Otomo, A.; Ho, Y.-L.; Delaunay, J.-J.; Nakano, Y.; Tanemura, T. Electrical tuning of metal-insulator-metal metasurface with electro-optic polymer. *Appl. Phys. Lett.* **2018**, *113*, 231102.

[2] Pors, A.; Nielsen, M. G.; Eriksen, R. L.; Bozhevolnyi, S. I. Broadband Focusing Flat Mirrors Based on Plasmonic Gradient Metasurfaces. *Nano Lett.* **2013**, *13*, 829–834.

[3] Boroviks, S.; Deshpande, R. A.; Mortensen, N. A.; Bozhevolnyi, S. I. Multifunctional Metamirror: Polarization Splitting and Focusing. *ACS Photonics* **2017**, *5*, 1648–1653.

[4] Park, S.; Lee, G.; Park, B.; Seo, Y.; bin Park, C.; Chun, Y. T.; Joo, C.; Rho, J.; Kim, J. M.; Hone, J.; Jun, S. C. Electrically focus-tuneable ultrathin lens for high-resolution square subpixels. *Light: Sci. Appl.* **2020**, *9*, 98.

[5] Shirmanesh, G. K.; Sokhoyan, R.; Wu, P. C.; Atwater, H. A. Electro-optically Tunable Multifunctional Metasurfaces. *ACS Nano* **2020**, *14*, 6912–6920.

[6] van de Groep, J.; Song, J.-H.; Celano, U.; Li, Q.; Kik, P. G.; Brongersma, M. L. Exciton resonance tuning of an atomically thin lens. *Nat. Photonics* **2020**, *14*, 426–430.